Report to Los Alamos National Laboratory: Measurements of Mica Crystal Bragg Reflections

September 5, 1996

M. L. Crow and A. Steyerl
Department of Physics
University of Rhode Island
Kingston, RI 02881

I. Introduction and Objectives

Goals of this work. An ultracold neutron converter using a mica crystal assembly as the Doppler reflector is under construction at the Los Alamos Neutron Science Center (LANSCE). The mosaic width and reflectivity of the crystal assembly are critical factors in the performance of the converter. Previous modeling [1] shows that the desired mosaic for the present configuration is ~3° in the scattering plane and small out of the scattering plane. The objective of this work is to examine the reflection characteristics of representative mica crystals, and to recommend a method for selecting and mounting mica crystals to make an efficient reflector.

Micas. Micas are layered, hydrated aluminosilicate minerals with the silicate tetrahedra arranged in two layers about a hydrated transition metal oxide octahedral plane, with alkali atoms (usually potassium) in the interplanar layers. Mica crystals have a characteristically large interplanar spacing, corresponding to the planar macroscopic structure. In particular, several micas have structures with a plane spacing (for the lowest order Bragg reflection) of about 9.6 to 10.1 Å [2,3]. Natural micas which are available as large crystals include muscovite, phlogopite (with a high Mg content), and biotite (with a high Fe content). Synthetic mica with fluorine substituted for the water molecules is synthesized commercially, but usually not in the form of large single crystals.

Other Studies of Mica:

Reflectors and Monochromators. Mica crystals have been used before as reflectors for ultracold neutron conversion, in the spallation source tested at Argonne [4,5]. In this case, synthetic fluorinated mica crystals were used as reflectors.

II. Mica Measurements

Measurement Methods. Rocking curves using a "standard" monochromator can give the shape and reflectivity of a crystal, but the results are strongly dependent on the collimation. Preliminary measurements on the mica crystals have been made using a two-axis spectrometer with a Cu (200) crystal monochromator. This gives some information on the shape of the mosaic, but the width of the Cu crystal used (~0.15° FWHM) limits the resolution. A reflectivity measurement is even less definitive, because the Cu apparently provides a larger wavelength spread than some of the mica crystals.

DISCLAIMER

DISCLAIMER

The use of two like crystals simplifies the analysis of the rocking curves [7] and improves the geometry for a reflectivity measurement. The results presented here come from measurements using two mica crystals. Triple axis spectrometers H7 and H4S at Brookhaven National Laboratory were used, each with a graphite monochromator, a mica crystal at the sample position (acting as a second monochromator), and a second mica crystal at the analyzer position. The measurement geometry is shown schematically in Fig. 1. For the sample position, a mica crystal with a narrow mosaic was selected. After rocking and tilting, this crystal was fixed at the maximum counting rate position, and used to provide a beam for measurements of a series of mica crystals at the analyzer position. Most of the two-crystal measurements were made in an antiparallel scattering geometry, which practically eliminated the contribution of the collimation to the observed rocking curve shape. In each case, the detector was set at the Bragg angle for the mica crystal at the analyzer position, and the crystal was rotated incrementally through the Bragg condition, and counted at each angle. For each crystal examined, the Bragg angle was varied to verify the 9.96 Å spacing value within about ±0.04 Å. A few transmission measurements were also made. This method gives the same rocking curve information with much poorer statistics, but it also provides a measure of the total attenuation by the crystal.

To obtain effective reflectivities, the peak and integrated intensities of the beam from the crystal at the analyzer position are compared to the peak and integrated intensities of the scattered beam from the crystal at the sample position. (The peak intensity is determined at the crystal setting with the highest counting rate; the integrated intensity is determined by integrating the counting rate over a series of angles as the crystal is rotated through the peak.) If the detector aperture is large enough to accept the entire scattered divergence, the interpretation is straightforward.

Results on mica crystals supplied by Los Alamos. The four mica crystals originally supplied by Los Alamos are described in Table I.

Table I. Parameters for the initial set of four mica crystals supplied by Los Alamos.

Supplier	Sample Material	Area Thickness
1. B & M Trading	Green Muscovite	6×6 cm^2 254 mm
2. B & M Trading	Ruby Muscovite	6×6 cm^2 254 mm
3. Perfection Mica	Ruby Muscovite	5.08 cm diameter 254 mm
4. Perfection Mica	Ruby Muscovite	7.62 cm diameter 79 mm

All of these natural crystals are very flat and free of scratches, and suitable for optical windows. The suppliers selected these specimens from mined mica for flatness and transparency, and cleaved and cut them for their primary commercial use as oven windows. The Perfection Mica Co. samples show no evidence of delamination at the edges. The B & M Trading Co. samples have minimal delamination near the square corners.

Each crystal was mounted at the analyzer position in eight different orientations. For the square crystals, this meant four different edges faced upward, for each face of the crystal. A small ink mark was used to align the circular pieces in a similar sequence. Measurements were made at wavelengths of 4.11 Å and 2.37Å.

At 4.11 Å, the difference in the rocking curves when the orientation of the crystals is changed is striking. The rocking curve could be a single peak with a Gaussian width of <0.2° in one direction, and a less defined, multiple peaked shape in another. Some representative curves are shown in Fig. 2. Moreover, in some cases the peak shape changed markedly when the opposite face of the crystal was turned toward the beam. This suggests immediately that the entire crystal volume does not contribute to the scattering, which is the expected result if primary extinction is appreciable. Table II shows the average, maximum, and minimum values for FWHM, peak reflectivity, and integrated reflectivity for the four crystals, as measured at 4.11 Å.

No.	FWHM	Peak Reflectivity (%)	Integrated Reflectivity (%)
1	0.178	2.0, 3.4	1.0
2	0.197	1.3, 1.9	0.7
3	0.153	0.59, 1.2	0.36
4	0.182	0.39, 0.55	0.27

At 2.37 Å, there is somewhat better correlation between the two faces of the crystal, but there is still a significant orientation dependence, as seen in Fig. 3. Table III summarizes the results of these measurements.

No.	FWHM	Peak Intensity (ct/10s)	Integrated Intensity (ct/10s)
1	0.227	1.4	1.2,1.3,0.98
2	0.243	1.3	1.1,1.3,0.93
3	0.276	0.52	0.47,0.78,0.34
4	0.232	0.36	0.36,0.54,0.20

Attenuation. Data for the total attenuation by the crystals were also obtained with the crystals near the Bragg condition. The measured attenuation corresponded to macroscopic cross sections of 0.7 to 0.9 cm^{-1} at 2.37 Å. The components of the attenuation are the coherent scattering cross section, which is directly connected to the reflectivity, the incoherent scattering cross section (due mainly to hydrogen), and the absorption (inversely proportional to velocity). The incoherent scattering is the largest component at short wavelengths, and is nearly independent of the wavelength. The calculated macroscopic incoherent cross section for muscovite is 0.69 cm^{-1}. The calculated macroscopic absorption cross section is 0.02 cm^{-1} at 2.37 Å, and .19 cm^{-1} at 17.3 Å. The measured attenuation ranges from the same to slightly higher than the calculated values, possibly indicating a small variation in water content.

Other Mica Crystals. For comparison purposes, rocking curve data has been collected for several other mica crystals, including some geological specimens from Ward's Scientific Establishment and some flat muscovite samples belonging to Brookhaven. Most of the geological specimens, which have not been through the selection process which yielded the high optical quality samples, have a macroscopic waviness that correlates with the rocking curve width. The rocking curves are almost all wider than those seen in the Los Alamos specimens. Generally, the "rough" crystals of similar dimensions give higher integrated reflectivity, and sometimes higher peak reflectivity.

The Brookhaven samples are flat, relatively thick (~0.5–1 mm) pieces of natural green muscovite. Although the thicker crystals are less optically transparent, the rocking curves and reflectivities for these are similar to those of the Los Alamos specimens.

Attempts were made to change the rocking curve shape, and the reflectivity, by mechanical deformation of some crystals. Mechanical deformation, by repeatedly bending a crystal until partial delamination occurs, will broaden the mosaic irreversibly. Such a process was used on a phlogopite crystal which already had a broad ~0.85° mosaic, and a ~3° mosaic was obtained. In the case of this crystal, however, primary extinction was probably already low, and the integrated intensity was unchanged.

Another approach is to start with a macroscopically wavy crystal and put it into a press to flatten it, which should essentially force a broadly distributed angular distribution into a narrower angular range. Using a press developed by L. Passell at Brookhaven [7] which has a silicon single crystal plate on the illuminated side, the flatness dependence of some crystal rocking curves was examined. A piece of phlogopite that had a width of more than 3° before flattening had a flattened rocking curve width of ~0.65° (Fig. 4). The integrated intensity in the rocking curve was not changed very much, but the peak intensity increased by more than a factor of two.

III. Discussion

Comparison of observed reflectivities to calculated values. The first four samples supplied by Los Alamos have narrow mosaics and low reflectivities. For comparison, reflectivities were calculated for an ideally imperfect muscovite crystal with similar rocking curve width, and for a perfect crystal. For the ideally imperfect crystal, with 0.25 mm thickness and 0.2° mosaic width, the expected peak reflectivity is ~13% at 2.37 Å and 70% at 17.3 Å. The leading term in the reflectivity is the ratio between the macroscopic coherent (i.e., Bragg) scattering cross section and the attenuation cross section; the latter is dominated by incoherent scattering from hydrogen. For a perfect crystal, the peak reflectivity value at 2.37 Å is ~2.7%, with a FWHM of ~0.0015° and a penetration depth of 5.5 mm; at 17.3 Å, the calculated reflectivity is ~13% with a FWHM of ~0.013° and a penetration depth of 0.67 mm. The predicted width for a perfect crystal is far smaller than the observed shapes of the actual samples , while the calculated peak reflectivity is higher than the values observed at 2.37 Å.

Possible methods of improving the reflectivity. The sample crystals can be viewed as a collection of large perfect domains; the width variability and structure within the rocking curves illustrates the angular variation between these domains. Good optical transmission properties appear to correlate with large domain size and low neutron reflectivity. The low reflectivity is essentially due to primary extinction, which reduces the effective scattering volume by multiple scattering within the domains. Although crystals with poorer optical qualities clearly have larger total reflectivity, in most cases this is coupled with a much larger mosaic spread.

To increase the effective scattering volume, it is necessary in mica to introduce disorder between the domains, especially in the interplanar direction. Bending or breaking crystals can reduce the area of the perfect domains, but because of the large structural anisotropy, the domain thickness along the interplanar axis is difficult to influence by this method. A possible strategy for achieving a high peak reflectivity is to start with a flat mica crystal, cleave it into much thinner pieces, and restack it, rotating the pieces with respect to their original positions. This would have the effect of "filling in" the angular space between the individual domains. Another possible approach is elastic bending of the crystals, which could introduce a continuous variation in the planar orientation.

Recommendations. For the initial tests of the crystal converter system, the window quality mica will produce predictable mosaic structure, but rather low reflectivities. The mosaic spread of these crystals seems to average from 0.15 to 0.2°; to form an assembly with a 3° mosaic in one dimension, about 15 crystals can be mounted with a 0.2° angular spacing. Flat crystals are needed if each crystal must stand alone, with small spacers. If, as suggested by Los Alamos, silicon crystal wedges are used to introduce the angular spread, the silicon can serve a dual purpose as spacer and flattener, allowing the use of wavier crystals or stacks of crystals in the assembly. It is clear that none of the crystals examined so far has a reflectivity which approaches 1, or even 0.5, at 17.3 Å. The search for better mica reflectors can take one or both of two paths. More natural mica crystals can be tried, using the cleaving and stacking techniques suggested above. In addition, the use of fluorinated synthetic mica crystals can be explored further. A low hydrogen mica would be necessary to achieve a reflectivity beyond ~70% at 17.3 Å.

References

1. M. L. Crow and A. Steyerl, "Optimization of Pulsed Spallation Source Doppler Converters for Ultracold Neutron Production," unpublished report to Los Alamos, April 1996.
2. S. W. Bailey, "Structures of Layer Silicates," in *Crystal Structures of Clay Minerals and their X-ray Identification*, ed. G. W. Brindley and G. Brown, Mineralogical Soc. Monograph 5, 1980.
3. International Tables for Crystallography, ed. A. J. C. Wilson, Vol. C, pp. 674–678, (1992).
4. T. W. Dombeck, J. W. Lynn, S. A. Werner, T. Brun, J. Carpenter. V. Krohn, and R. Ringo, Nucl. Instrum. Methods **165**, 139 (1979).
5. T. O. Brun, J. M. Carpenter, V. E. Krohn, G. R. Ringo, J. W. Cronin, T. W. Dombeck, J. W. Lynn, and S. A. Werner, Phys. Lett. A **75**, 223 (1980).
6. U. Wildgruber and L. Passell, private communication.
7. M. J. Cooper, Acta Cryst. A **24**, 624 (1968).

May 1, 1996

Report to Los Alamos National Laboratory on Optimization of Pulsed Spallation Source Doppler Converters for Ultracold Neutron Production

M. L. Crow and A. Steyerl
Department of Physics
University of Rhode Island
Kingston, RI 02881

Abstract. This report describes a design optimization study for Doppler conversion ultracold neutron (UCN) production devices for pulsed spallation source. The primary focus here is a computer simulation of a mica crystal reflection device to be installed at the short-pulse spallation source at Los Alamos National Laboratory [1]. This simulation is an extension of our work on a concept for a multilayer reflector Doppler turbine converter for a long–pulse spallation source [2]. In addition to the simulation of the presently planned configuration, possible modifications which could improve converter performance are examined, and a comparison is made between crystal and multilayer reflectors.

1. ***Introduction.*** In a Doppler converter for ultracold neutron (UCN) production, neutrons from a segment of the cold neutron spectrum reflect from a receding blade, so that the resultant velocity in the laboratory frame is near zero. Multiply reflecting turbines based on continuous reactor sources have been used as effective UCN sources [3,4,5]. Pulsed spallation sources offer peak source currents comparable to and potentially greater than the best available reactors at high pulse repetition rates. For pulsed sources, single reflection Doppler converters offer the possibility of using the time structure to produce UCN efficiently. The use of crystal UCN converters has been examined before [6, 7] and a prototype was tested on a pulsed source at Argonne [8]. The present work extends the recent analysis of a single reflection turbine using multilayer reflectors [2] on a long-pulse spallation source (such as that proposed for Los Alamos [9,10]) to a UCN source using mica crystal reflectors, under development at Los Alamos [1] for use at the present short-pulse source [11].

When producing UCN from a pulsed primary source, the Doppler conversion method has two important advantages over a direct UCN extraction tube. The first is the higher extraction efficiency for cold neutrons, which can pass through guides with a small number of reflections, and penetrate the material windows necessary for a cryogenic moderator system with little attenuation. In contrast, UCN undergo many more reflections, and are severely attenuated by back-reflection and absorption in windows. The second advantage, which is essential to achieving a high extraction efficiency when the primary neutron source is pulsed, is that the extraction of cold neutrons is fast enough that the conversion can take place *before* the neutrons are spread out in time, so that it is possible to convert neutrons from the peak phase space density of the source to ultracold neutron velocities.

The performance of the ultracold neutron source is best characterized in terms of the exit phase space density of a Doppler converter, which is limited by Liouville's theorem to the peak neutron density of the primary source. The peak current at the velocity chosen for conversion determines the peak achievable UCN source *density*. To obtain a high *rate* of UCN production, the converter must be designed to fill the UCN velocity space volume. In addition, the output area should be as large or larger than the feeding guide area, and the output pulses should fill as much of the available time as possible.

The flight path distance and the primary pulse duration are closely coupled to the velocity bandwidth selected for conversion. For longitudinal velocities (along the direction of the feeding guide), the spreading time Δt_{spread}, which is the separation in time of two velocities v + Δv and v – Δv after a flight distance L, is given by

$$\Delta t_{spread} = 2\, L\, \Delta v \,/\, v^2. \quad (1)$$

If Δt_{spread} is greater than the primary pulse length Δt_{pulse}, the highest and lowest velocities are resolved, and the entire velocity band is not available for conversion by the reflector. The effective spread in velocity arriving at a converter can be expressed as

$$\Delta v = \Delta t_{pulse}\, v^2 \,/\, 2\, L\, . \quad (2)$$

Since the velocity spread in the directions transverse to the feeding guide is defined by the guide critical velocity, the longitudinal velocity spread may be the narrowest. For the present Los Alamos design, with an 8 m flight path, 0.200 ms pulse length, and incident velocity of 395 m/s, Δv is 1.95 m/s, much smaller than the 7.6 m/s critical velocity for the ^{58}Ni feeding guide.

2. ***Planned Source at Los Alamos.*** *Primary source, guide, and velocity drive.* The source under development at Los Alamos [1] will use a liquid hydrogen Cold Source, with a pulse width of about 0.2 ms at 400 m/s, as the primary source. The repetition frequency of this source is 20 Hz. In the current design, the feeding guide starts about 1 m from the moderator and is 7 m long, for a total source-to converter distance of 8 m. The square guide is 6×6 cm^2 and has a ^{58}Ni surface. The feeding guide enters the rotor housing within the rotation plane at an inclination of 28.8° to the tangent (the same feeding geometry as the Argonne source). The rotor has a radius of 0.90 m and will run at 40 Hz, with a peripheral speed of ~ 226 m/s. The reflector mounting has a 28.8° tilt from the radius to match the feeding guide angle.

Crystal Reflector. The currently planned reflector material is muscovite, a widely available natural mica. The d-spacing of the lowest order reflection is ~ 9.96 Å, which sets the incident neutron velocity to 395 m/s. The typical mosaic width, reflectivity, and attenuation of the natural crystals requires further investigation. The mosaic can be broadened to a large value by stacking crystal plates with wedges, but attenuation is a potential problem for a large number of layers. An alternate material also under consideration is a hydrogen-free synthetic mica, fluor-phlogopite, with a similar d-spacing. The reflectivity of this material has been measured to be ~30% at 2.3 Å for a 0.25 mm thick crystal with a mosaic of .08° [12, 13]; the reflectivity should be higher, for thinner plates, at 21 Å (197 m/s). Although this material should have lower attenuation than the natural mica, it has the disadvantages of high cost and limited availability of large crystals of uniform thickness.

UCN exit and shutter. In the Los Alamos design, the UCN exit axially through a rotary shutter. The axial exit has the advantage of providing a short distance from the blade path to the exit guide. The function of the shutter is to reflect UCN which escape from a bottle attached to the exit guide between UCN output pulses, so that the peak source density can be approached within the bottle. If the shutter has one opening, the rotational velocity is ~18 m/s at the center of the exit.

3. ***Simulation of a Crystal Converter.*** The simulation program for a UCN Doppler converter using a multilayer reflector at a long–pulse spallation source [2] has been adapted to simulate a converter with a crystal reflector at a short-pulse spallation source. The program has been modified to use an in-plane feeding guide; otherwise the feeding guide, timing, blade motion, and UCN exit features are identical. The most important change in the program is the substitution of a mosaic crystal reflector for a broad-band multilayer.

The input neutron distribution for the program is taken to be Maxwellian in the Cold Source, and to be distributed over a pulse length Δt_{source} ; the time dependence of a particular Cold Source may be used. The program models the paths of the neutrons through the guides from the Cold Source to the turbine, and through the turbine to the UCN exit. When a neutron intercepts the walls of a guide, specular reflection is assumed if the normal velocity is less than the critical velocity of the guide; otherwise the neutron is lost in the guide wall (*i. e.* over-critical reflection is neglected). Sub-critical reflectivity of 99% is assumed, neglecting the linear dependence on the angle of incidence for roughness induced reflection losses [14]. The effects of gravity, guide gaps, and the attenuation by transmission windows are included, as in Crow *et al.* [15, 2]. Guide length and material are parameters of optimization. The time of passage through the guides is calculated to obtain the arrival time of each trial neutron at the turbine blade.

The turbine section of the program simulates the interaction of each trial neutron with the turbine blade. The neutron reflection process is calculated in the moving and accelerating frame of the turbine blade, taking into account the effects of centrifugal and Coriolis accelerations. In the rotating frame of the crystal reflector, the program determines the angle of incidence on the crystal and the Bragg angle corresponding to the incident neutron velocity. The angle of incidence is compared to the center of the reflector mosaic to determine the probability of reflection. The Bragg angle is then used to calculate the reflected velocity of each neutron. The program currently uses a Gaussian mosaic model characterized by a peak reflectivity and a width; an experimental rocking curve may be entered in place of the Gaussian.

The results are tabulated in the laboratory frame, as a function of position, velocity, and time, at one side of the turbine for the axial exit geometry. The phase space efficiency is calculated for selected phase space volumes.

4. ***Simulation Results.*** The calculations indicate the shape of the exit velocity space volume, which is effectively determined by the incident velocity space volume. The widths in the three velocity directions are illustrated in Fig. 1. The velocity widths of the UCN "cloud" in the directions perpendicular to the incident beam direction are given approximately by the critical velocity of the incident guide. The axial component, which is perpendicular to the scattering plane, is broadened somewhat by the out-of-plane mosaic. There is no advantage to artificially broadening the mosaic in this direction. The velocity width in the direction within the scattering plane and perpendicular to the incident beam is nearly equal to the guide velocity width at any point, but is spread out by the circular reflector motion when averaged over the exit area.

Dependence on crystal mosaic. The velocity width along the incident beam direction is determined mainly by the spreading of the neutron pulse along the flight path. The velocity width is about +/- 2 m/s for the 8 m flight path. The efficiency has a clear dependence on the mosaic spread within the scattering plane. Calculations as a function of mosaic spread (Fig. 2) show that a width up to ~3° is useful (with the 0.2 ms pulse and 8 m flight path), if the reflectivity can be kept constant. With a shorter flight path or a longer pulse, the maximum efficiency would require a larger mosaic width Table I shows some results, with a peak crystal reflectivity of 50%. The calculations shown here have been performed using this value based on the reflector discussion of Dombeck *et al.* [6]; the dependence of the efficiency on the reflectivity is linear. The efficiency is evaluated for a "box" in velocity space of $2.6 < v_{axial} < 7.6$ m/s in the axial direction, and $-7.6 < v < 7.6$ m/s in the other two directions, a 5×8 cm^2 exit area, and an 11 ms output pulse length.

Table I. Phase space conversion efficiency versus horizontal mosaic width for the Los Alamos geometry, with a 0.2 ms pulse and 8 m flight path.

EtaC (radians)	Mosaic FWHM (degrees)	Efficiency
0.002	0.27	0.0048
0.005	0.67	0.0119
0.010	1.35	0.0192
0.015	2.02	0.0208
0.020	2.70	0.0231
0.025	3.37	0.0241
0.030	4.05	0.0247
0.050	6.75	0.0252
0.100	13.50	0.0257

The UCN at the exit are spread over an area only slightly larger than the incident guide cross section; the exit area is about 6 cm wide and 10 cm high

FWHM. The widths are illustrated in Fig. 3. The overall distribution is broadened in the vertical direction as a result of the circular motion of the blade, .

Timing. The UCN pulse starts during the blade interaction with the beam, which for the 8 m guide path and 395 m/s velocity, starts ~20.74 ms after the primary pulse, as shown in the timing diagram (Fig. 4). The full width at half maximum of the UCN pulse, determined mainly by the reflector width along the exit direction, is about 11 ms. This is about one-fifth of the 50 ms pulse interval, so that this must be considered as a pulsed rather than a "quasi-continuous" UCN source. This exit width determines the optimum shutter opening time.

The dependence of the efficiency on the blade arrival time was examined to establish the synchronization requirements. The results (Fig. 5) show a curve with a FWHM of about 0.30 ms.

Calculated velocity distributions for time-of-flight. In practice, the performance of a converter has been measured by performing a time-of-flight measurement on UCN in the exit guide [3, 4, 8]. For comparison purposes, we have calculated the output of the Argonne converter (Fig. 6), which compares well with the measured shape of its output [8]. The expected output for the Los Alamos apparatus, shown in Fig. 7, has a much narrower velocity distribution because the beam is not broadened significantly in the axial direction. This also results in a higher conversion efficiency for neutrons with $v_{axial} < 7.6$ m/s.

5. ***Discussion and Possible Modifications.*** The basic characteristics of the Los Alamos rotor converter as presently designed have been modeled, and a dependence on the (not yet finalized) crystal mosaic is being compiled. The efficiency is limited by the incomplete velocity space filling in the longitudinal direction, which could in principle be increased by a factor of four. The total

current is also limited by the time filling of the output pulse. Some changes in the apparatus which could increase the efficiency or the current can be considered.

Mirror opposite exit. A method of using UCN with the "wrong" axial velocity direction is to place a neutron mirror opposite the exit, such that the reflected neutrons move toward the exit. This approach has the advantage that it would require no changes in the feeding guide or the blade size to implement it within the present plans. A simulation with a flat ^{58}Ni mirror (Fig. 9) indicates that the resultant pulse has a primary component (identical to the pulse with no mirror) and a reflected pulse which is later, longer, and lower in peak intensity. The loss in intensity is due to time spreading and to the increase in exit area. Although the much longer (~ 25 ms) pulse has a somewhat reduced average efficiency, the increase in the number of UCN per pulse at the exit approaches a factor of two.

Crystal tilt and guide divergence. The possibility of tilting the crystal to introduce an axial bias velocity has been examined. The enhancement of efficiency is small, because the UCN velocity region is already nearly filled in the axial direction. A bias velocity would be more effective if a divergent guide was introduced to narrow the velocity, and a wider reflector was used. This would have the effect of lengthening the UCN pulse, while maintaining much of the conversion efficiency; the additional current comes from using a larger fraction of the transverse velocity spread. The main drawback is the need for a larger blade. This divergent guide approach was used in the long–pulse turbine concept [2]. The main drawback of the divergent guide approach is the need to increase the reflector area; such an area increase may be less difficult with a low velocity supermirror than with a crystal.

Either the mirror or the divergent guide would require an increase in the shutter opening time, because of the increased pulse length. A combination of the two (possibly using a supermirror feeding guide) could produce a pulse comparable to the 50 ms pulse interval, eliminating the need for the shutter.

Shortening flight path / increasing pulse length. For the existing spallation source, there are strong constraints on the flight path distance and the source pulse length. Within these constraints, moving the UCN source to a position closer to an equivalent Cold Source, with a 0.2 ms effective pulse length, will produce a nearly linear improvement in the efficiency. (The distance for 395 +/- 7.6 m/s velocity at the crystal is ~ 2 m for this pulse length, a location well within the bulk shield.) An increase of the effective pulse length, as is possible by the use of a coupled Cold Source, would also increase the conversion efficiency.

Comparison of short-pulse crystal converter with long-pulse converter possibilities. As noted above, the crystal converter designed for the Los Alamos short-pulse source would have a larger incident velocity volume with a long-pulse source primary pulse of around 1 ms, by a factor of ~ 4 for the velocity "box" defined in section 3, given the same flight path distance. This would lead to a proportionally higher efficiency if the crystal mosaic could be broadened (also by a factor of 4) without loss of reflectivity. The multilayer converter which has been proposed for use with long-pulse sources [2] requires a shorter flight path because of the lower incident neutron velocities (less than 200 m/s for multilayer spacing greater than 20 Å). A lower blade speed reduces the distance traveled by the blade during the pulse interaction, which reduces the angular change during the interaction. The central parameter in choosing between crystal and multilayer reflectors for a long-pulse source, however, is the reflectivity across a sufficiently wide velocity band and area.

6. ***Conclusions.*** *Presently planned short-pulse crystal source at Los Alamos.* The mica crystal short-pulse source presently under development at Los Alamos will convert cold neutrons to UCN with a phase space efficiency of about 2.4% with a crystal mosaic of at least 3° FWHM, assuming 50% reflectivity. If it is likely that the apparatus may be moved to a shorter flight path or to a coupled moderator in the future, a wider mosaic would be needed to realize an efficiency improvement. There is a clear need for additional data on mica reflectivity, mosaicity, and transmission in order to complete the reflector design. The transmission of the natural mica in particular is needed to determine whether a sufficient mosaic spread can be achieved by stacking crystals. The back-reflection mirror would be a straightforward modification to the current design, and the large current increase should offset the small decrease in average density.

Future Doppler conversion UCN source for a long-pulse spallation source. It is clearly possible geometrically to produce a quasi-continuous source with a high conversion efficiency by using a combination of a divergent guide and back-reflection. The principal technical issue in using a long-pulse source effectively is the availability of reflectors with sufficient velocity band width *and* reflectivity. The candidates for these reflectors, mica crystals and multilayers, both require further measurements. Even if natural mica can be used effectively in the short-pulse source, low transmission could be a more serious problem with the wider mosaic (possibly > 10°) required for the long-pulse source. The small lattice spacing multilayers suggested as alternatives [2], such as W - $^{11}B_4C$, offer more options for large areas with high reflectivity and a large velocity width acceptance, but such multilayers have not yet been made, and their use would require a development program for fabrication and characterization.

References

1. T. J. Bowles, *Ultracold Neutron Workshop,* Santa Fe, NM, 1995.
2. M. L. Crow, L. Esibov, and A. Steyerl, submitted to Nucl. Instr. and Meth. A, 1996.
3. A. Steyerl, Nucl. Instr. and Meth. **125**, 461 (1975).
4. A. Steyerl, H. Nagel, F.-X. Schreiber, K.-A. Steinhauser, R. Gähler, W. Gläser, P. Ageron, J. M. Astruc, W. Drexel, R. Gervais, and W. Mampe, Phys. Lett. A **116**, 347 (1986).
5. M. Utsuro, T. Ebisawa, K. Okumura, S. Shirahama, and Y. Kawabata, Nucl. Instr. and Meth. **270**, 456 (1988).
6. T. W. Dombeck, J. W. Lynn, S. A. Werner, T. Brun, J. Carpenter, V. Krohn, and R. Ringo, Nucl. Instr. and Meth. **165**, 139 (1979).
7. C. F. Majkrzak and S. S. Malik, J. Appl. Cryst. **13**, 265 (1980).
8. T. O. Brun, J. M. Carpenter, V. E. Krohn, G. R. Ringo, J. W. Cronin, T. W. Dombeck, J. W. Lynn, and S. A. Werner, Phys. Lett. A **75**, 223 (1980).
9. J. Alonso, R. Pynn, T. Russell, and L. Schroeder (eds.), "Proceedings of the Workshop on Neutron Instrumentation for a Long–Pulse Spallation Source", Lawrence Berkeley National Laboratory Workshop Proceedings LBL–37880 (1995).
10. J. C. Browne, R. Pynn, and D. J. Weinacht (eds.), "A Long–Pulse Spallation Source", Los Alamos National Laboratory Report LA–UR–95–2760 (1995).
11. R. N. Silver, Physica B **137**, 359 (1986); P. W. Lisowski, C. D. Bowman, G. J. Russell, and S. A. Wender, Nucl. Sci. and Eng. **106**, 208 (1990).
12. C. F. Majkrzak, private communication (1996).
13. L. Passell, private communication (1996).
14. A. Steyerl, Z. Phys. **254**,169 (1972).
15. M. L. Crow, A. Steyerl, John B. Hayter, and T. J. McManamy, Nucl. Instr. and Meth. A **355**, 484 (1995).

Figure Captions

Figure 1. Velocity distribution of UCN, averaged over the axial exit area. (a) Velocity distribution in the longitudinal direction, parallel to the feeding guide, with a FWHM of 4 m/s. (b) Velocity distribution in the axial direction, with a FWHM of about 6 m/s. The distribution in the opposite direction is similar. (c) Velocity distribution perpendicular to the feeding guide and the rotation axis, with a FWHM of > 20 m/s. The large width is a consequence of circular blade motion.

Figure 2. Dependence of the conversion efficiency (referenced to the phase space density in the Cold Source) on the crystal mosaic for the Los Alamos converter design. The crystal model used here is a mica crystal (d=9.96 Å) with a constant peak reflectivity of 0.5 and a variable Gaussian mosaic width η_C. The primary pulse length is 0.2 ms, the flight path length is 8 m , and the output pulse length is 11 ms.

Figure 3. Position distribution of UCN (between 2.6 and 7.6 m/s) at the axial exit plane. (a) Longitudinal distribution, with a FWHM of ~ 5 cm. (b) Transverse distribution, with a FWHM of ~ 8 cm.

Figure 4. Timing diagram for the Los Alamos converter. (a) Primary pulses have a 20 Hz frequency. (b) The flight time is ~ 20.7 ms. (c) The interaction time is about 0.5 ms. (d) The UCN output pulse time, for axial velocity 2.6 m/s $< V_{axial} < 7.6$ m/s. The FWHM is about 11 ms.

Figure 5. Dependence of the conversion efficiency on the value of $\Delta t_0 t$, where $t_0 t$ is the arrival time of the blade at the center of the incident beam path, referenced to the primary pulse time.

Figure 6. Counts versus longitudinal velocity along the exit guide of the Argonne UCN converter [7]. The calculation using the present simulation gives a comparable velocity width.

Figure 7. The calculated velocity distribution for an axial guide using the current Los Alamos design. The velocity distribution is much narrower in this direction than in the Argonne guide, and the expected efficiency is more than a factor of two higher.

Figure 8. Timing diagram for the Los Alamos converter with a flat 58Ni back reflecting mirror opposite the UCN exit. Although the average efficiency is lower than with the "direct" pulse alone, the number of UCN (between 2.6 and 7.6 m/s) is increased by nearly a factor of two.

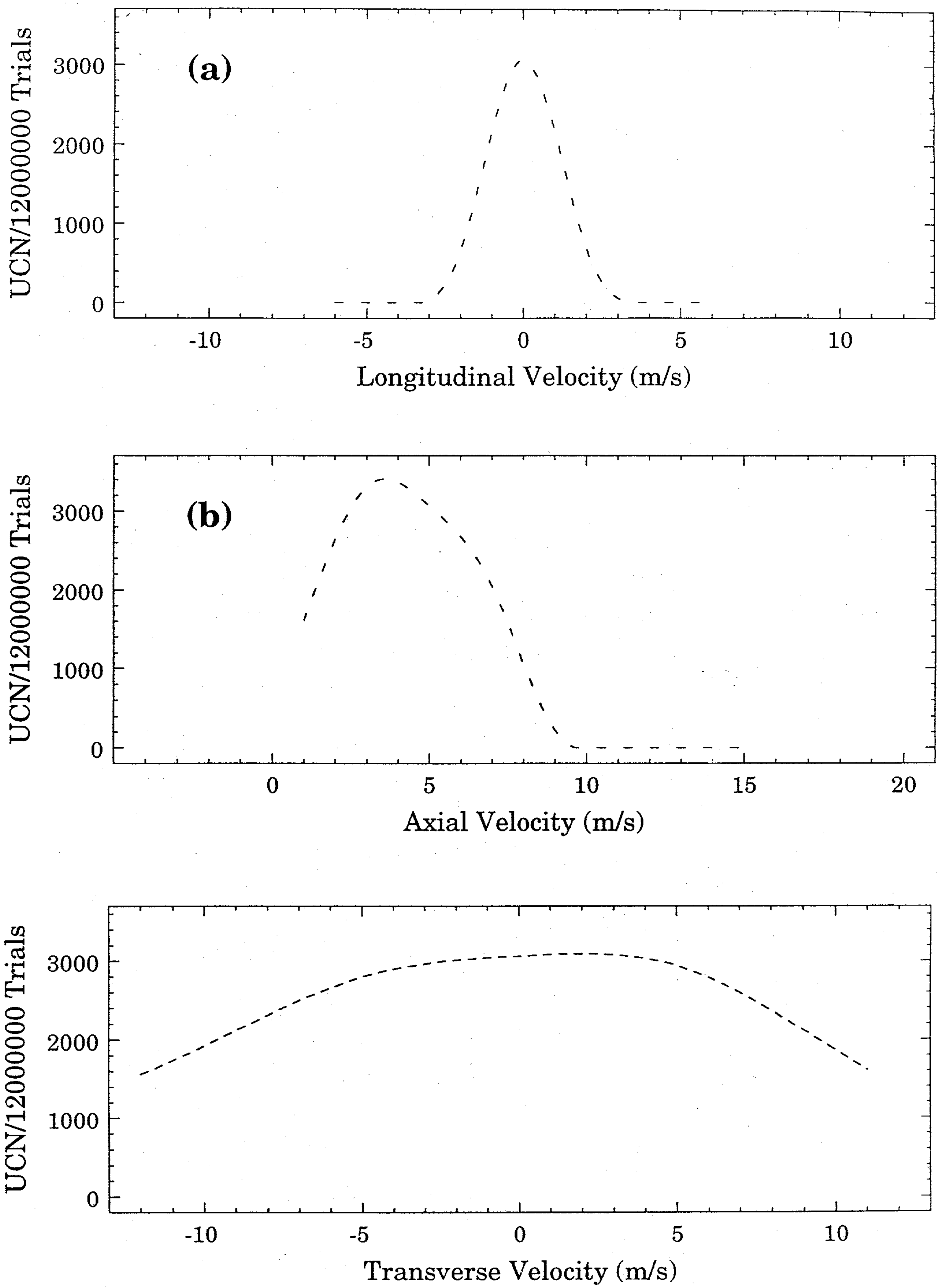
UCN/12000000 Trials
3000
2000
1000
0
(a)
-10
-5
0
5
10
Longitudinal Velocity (m/s)
UCN/12000000 Trials
3000
2000
1000
0
(b)
0
5
10
15
20
Axial Velocity (m/s)
UCN/12000000 Trials
3000
2000
1000
0
-10
-5
0
5
10
Transverse Velocity (m/s)

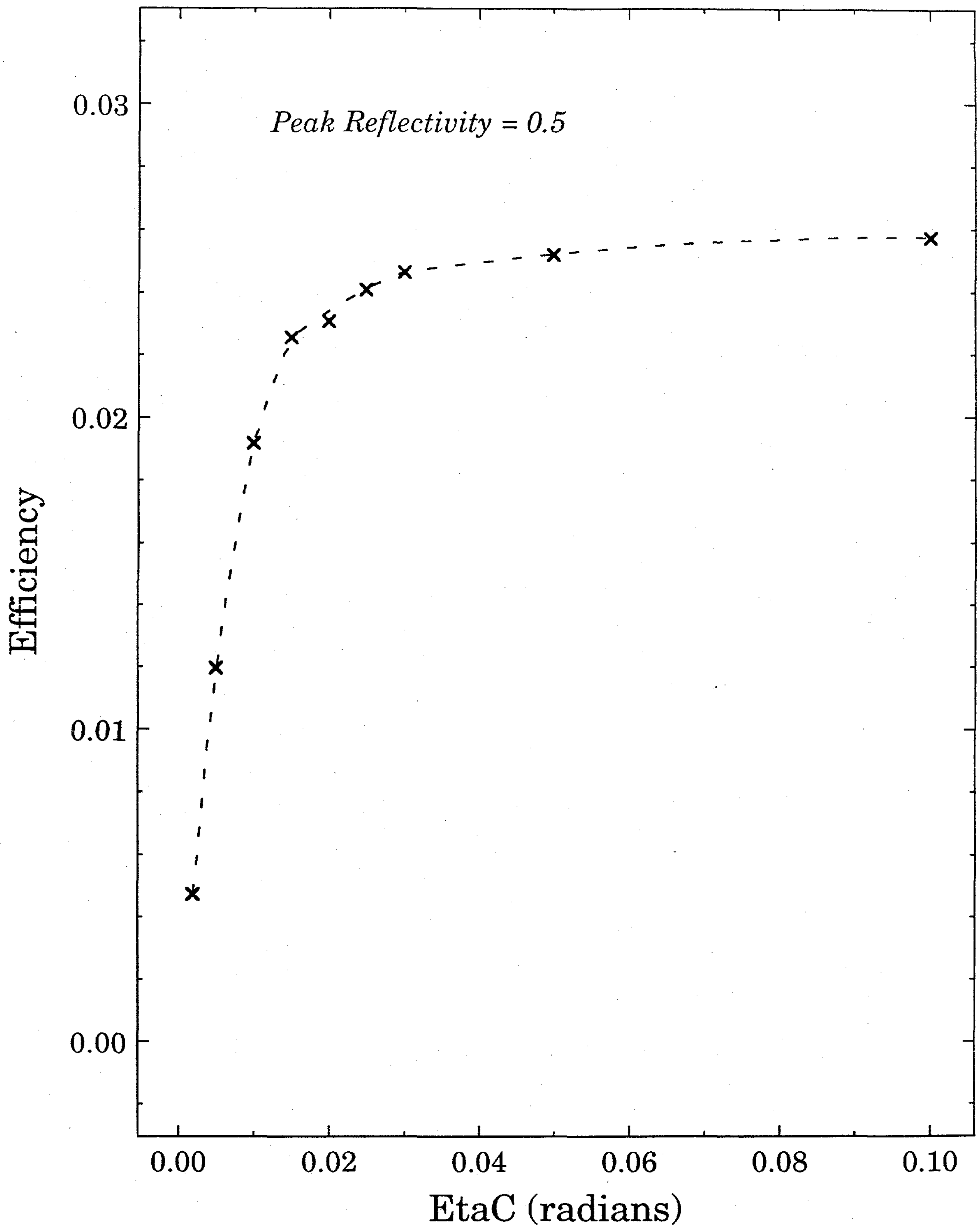
Peak Reflectivity = 0.5
Efficiency
0.03
0.02
0.01
0.00
0.00
0.02
0.04
0.06
0.08
0.10
EtaC (radians)

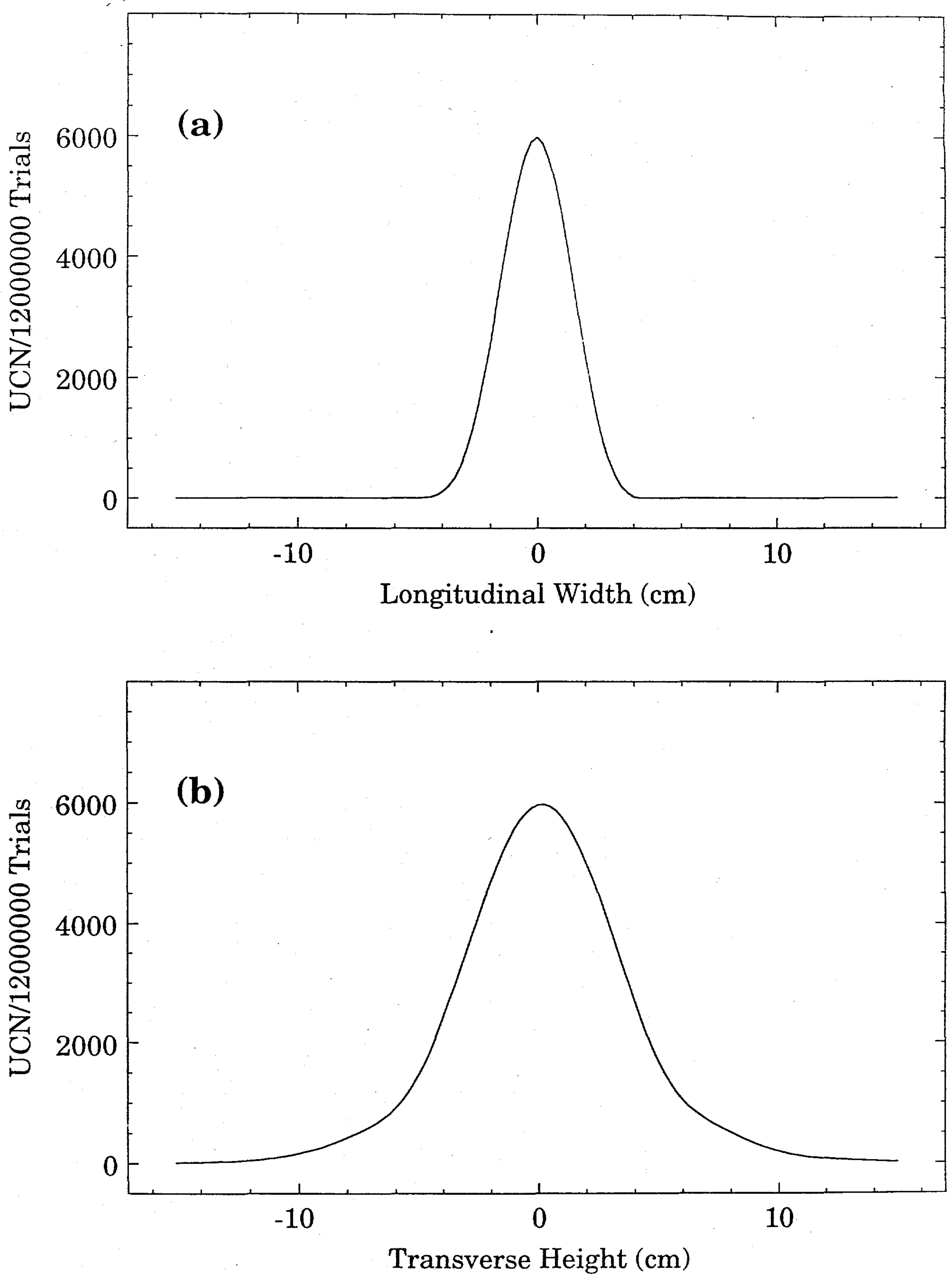
(a)
UCN/12000000 Trials
6000
4000
2000
0
-10
0
10
Longitudinal Width (cm)
(b)
UCN/12000000 Trials
6000
4000
2000
0
-10
0
10
Transverse Height (cm)

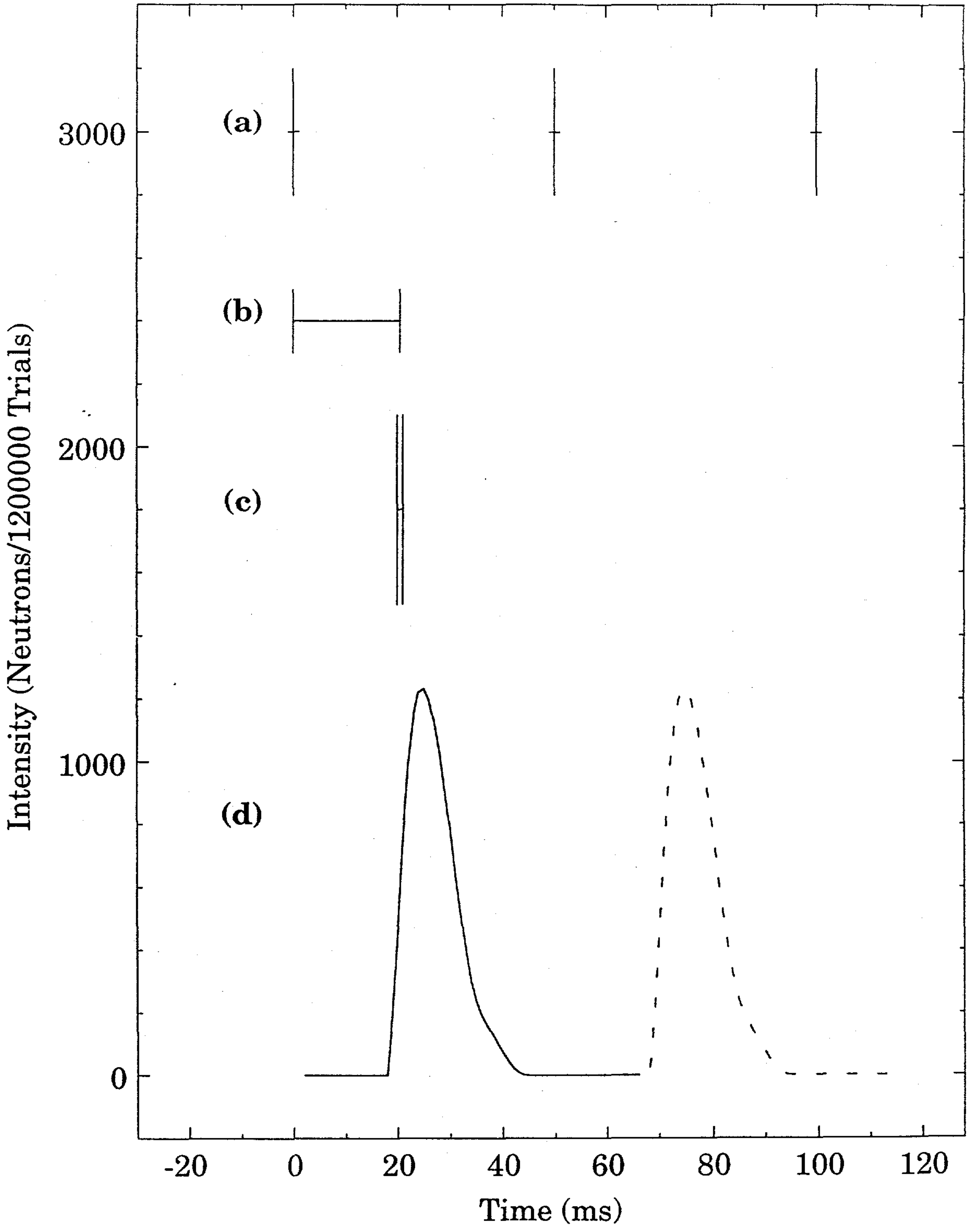
(a)
(b)
(c)
(d)
3000
2000
1000
0
Intensity (Neutrons/1200000 Trials)
-20
0
20
40
60
80
100
120
Time (ms)

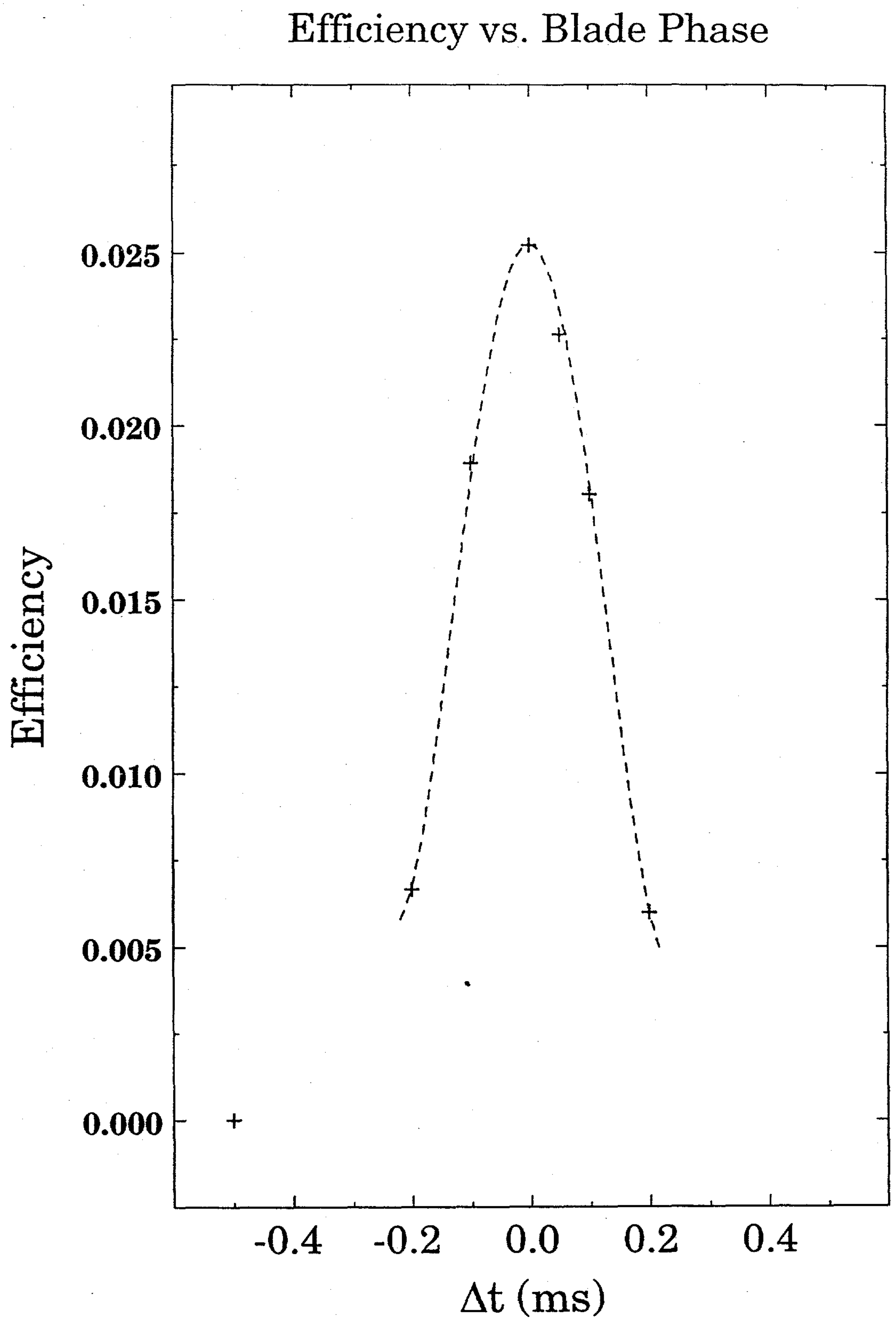
Efficiency vs. Blade Phase
Efficiency
0.025
0.020
0.015
0.010
0.005
0.000
-0.4
-0.2
0.0
0.2
0.4
Δt (ms)

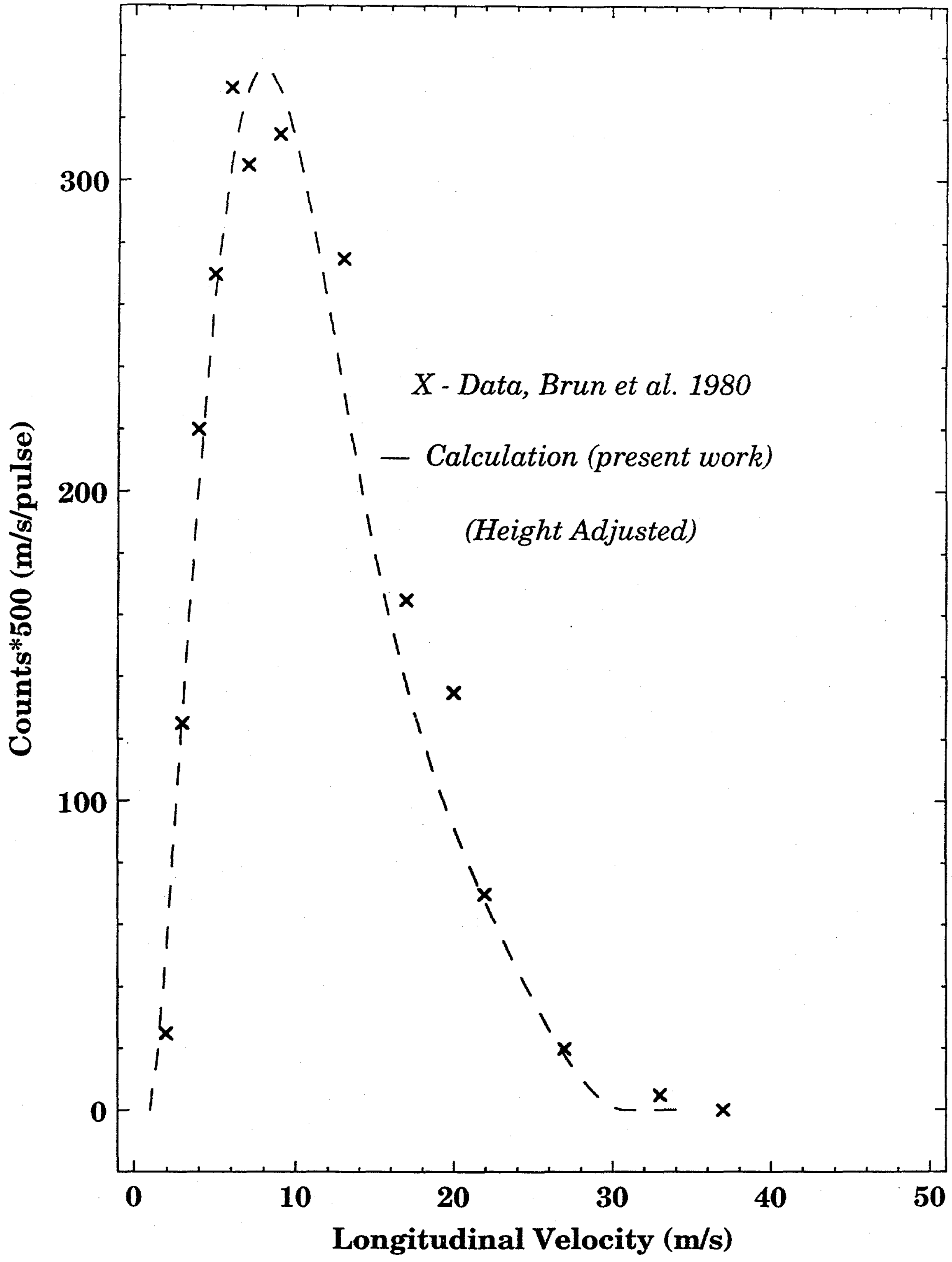
X - Data, Brun et al. 1980
— Calculation (present work)
(Height Adjusted)
Counts*500 (m/s/pulse)
Longitudinal Velocity (m/s)
0
100
200
300
0
10
20
30
40
50

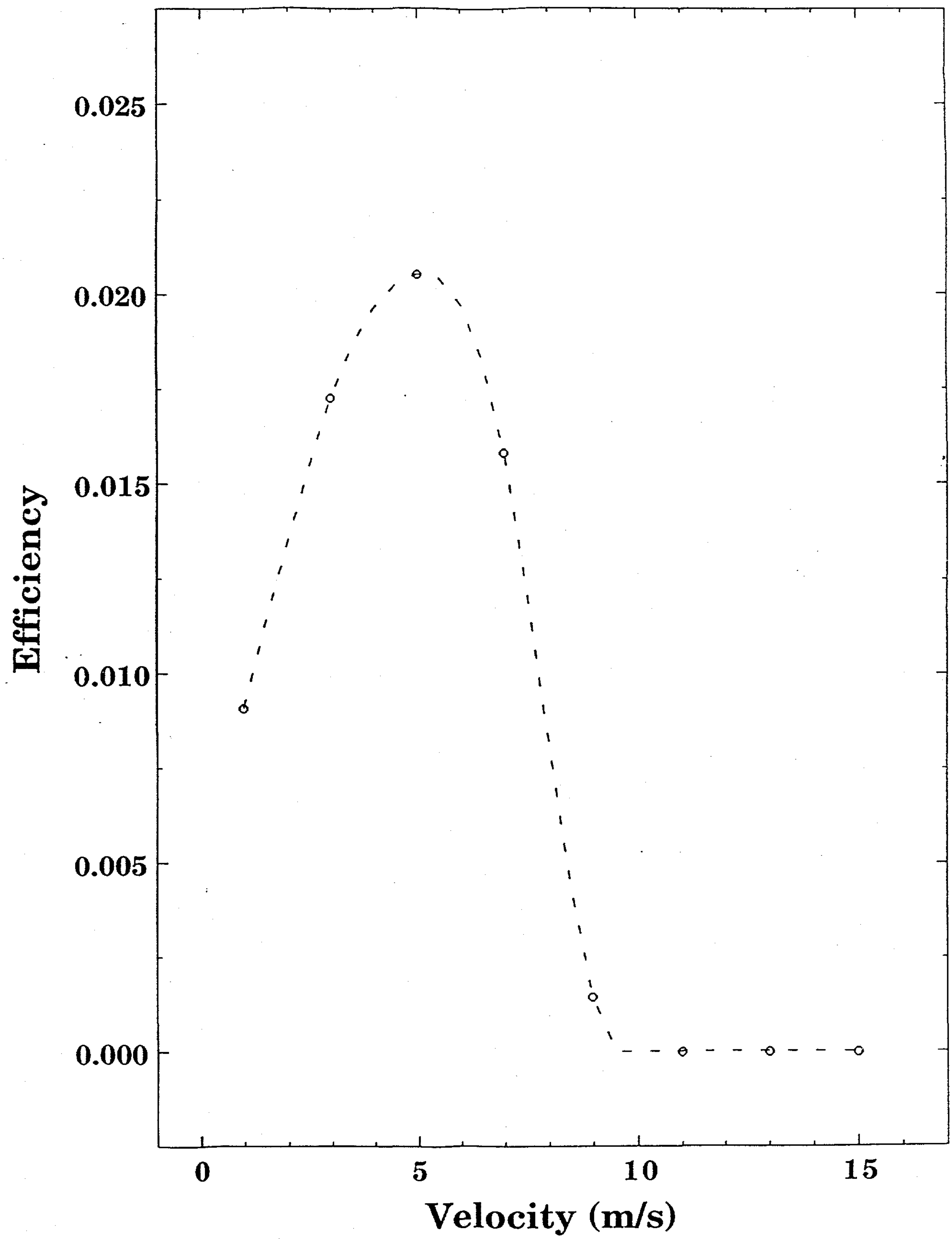
0.025
0.020
0.015
0.010
0.005
0.000
Efficiency
0
5
10
15
Velocity (m/s)

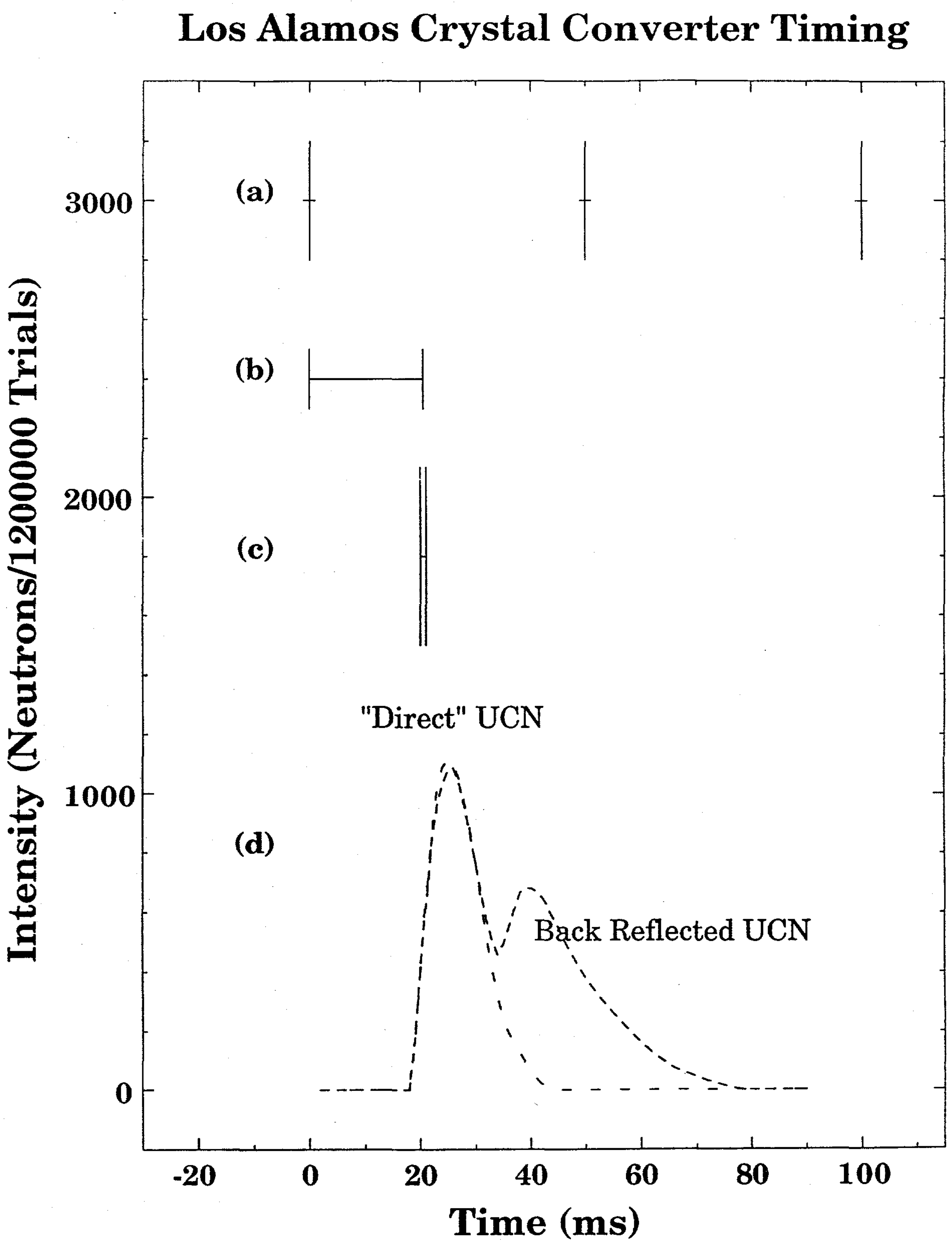
Los Alamos Crystal Converter Timing
Intensity (Neutrons/1200000 Trials)
3000
2000
1000
0
(a)
(b)
(c)
(d)
"Direct" UCN
Back Reflected UCN
-20
0
20
40
60
80
100
Time (ms)